10.2514/6.2016-0078

AIAA SciTech Forum
4-8 January 2016, San Diego, California, USA
54th AIAA Aerospace Sciences Meeting

Response of a shock train to downstream back pressure forcing

Robin L. Klomparens* , James F. Driscoll† , and Mirko Gamba‡
University of Michigan, Ann Arbor, MI 48109

Schlieren movies and pressure measurements are collected to analyze the response of a shock train due to downstream pressure forcing. The shock train is generated in a Mach 2.0 ducted flow and controlled by a downstream butterfly valve. Cyclic opening and closing of the valve leads to an oscillatory motion of the shock train and subsequent oscillations in back pressure measured at the end of the duct. Different cases of forcing frequency are studied. In all of the cases there is a clear hysteresis effect that causes the shock train to travel along a different path for the upstream and downstream movements. Increasing the forcing frequency leads to a smaller difference between limiting values of the back pressure and shock train position during the oscillatory process. However, when properly normalized the different cases follow the same path and thus only depend on the history of back pressure. Finally, the shock speed is decomposed into low frequency (bulk) and high frequency components. The magnitude of the high frequency component is larger but does not show the oscillatory motion of the shock train. The extrema values of the bulk speed are independent of forcing frequency but the time history of speed during a cycle is not.

Nomenclature

t	Time
x	Coordinate in the streamwise direction
y	Coordinate in the transverse direction
z	Coordinate in the vertical direction
p_b	Back pressure (measured at x=1011 mm)
Θ_1	Initial valve angle
Θ_2	Final valve angle
$\dot{\Theta}$	Rate of change of control valve angle
Δt	Duration of time spent at each valve angle
Ω	Forcing frequency $= 1/(2\Delta t)$
τ_x	Time delay between the signals of valve angle and shock train position
τ_p	Time delay between the signals of valve angle and back pressure
T_x	Rise time of shock train position signal
T_p	Rise time of back pressure signal
x_I	x-location of the leading shock intersection point
u_I	Velocity of the leading shock in the shock train
U_I	Bulk velocity of the leading shock (u_I lowpass filtered at 50 Hz)

Symbols

$X^\star$	Average initial value before back pressure forcing ($t < \Delta t$)
$X^\pm$	Maximum/minimum value for a given case

*Graduate Research Assistant, Dept. of Aerospace Engineering, AIAA member.
†Arthur B. Modine Professor, Dept. of Aerospace Engineering, AIAA member.
‡Assistant Professor, Dept. of Aerospace Engineering, AIAA member.

I. Introduction

A shock train is a sequence of shock and compression waves that gradually decelerates a supersonic flow. The resulting shock pattern is highly three-dimensional with multiple shock-wave boundary-layer interactions (SBLI). Shock trains are extremely relevant in air-breathing propulsion systems because they are the critical elements in isolators of high-speed air-breathing engines, such as ramjet and scramjets. In these engines, the flow captured by the inlet passes through the shock train where it is slowed down and compressed before entering the combustor. If the isolator is long enough, a mixing region will exist where shocks are not present but pressure continuously rises due to mixing between the supersonic and subsonic regions of the core flow. The entire region from the beginning of the shock train to the end of the mixing region is known as a pseudo-shock.[1]

In an actual engine, the pressure rise in the combustor sustains the shock train. However, if the back pressure is too large for the shock system to compensate for, then the shock system propagates upstream until it is disgorged from the inlet. This transient process is known as inlet unstart. When the shock train is ejected, a bow shock forms outside of the inlet leading to flow spillage and reduced mass flow rate through the engine. As a consequence, there is loss of engine thrust, significantly increased loads, and intense oscillatory flow.[2–4]

During the typical operation of a high-speed air-breathing engine within the flight envelope, the combustor undergoes different transient combustion processes. For example, the initial ignition process and changes in fueling scheme (e.g., fueling rate, position, etc.) may be experienced as the vehicle follows the desired trajectory. These transient combustion phenomena induce changes in the combustor pressure and subsequently alter the shock train in the isolator such that the incoming flow conditions can be processed by the shock train to match the new combustor conditions. It is therefore important to understand the dynamics of shock trains when perturbed by downstream forcing, such as the pressure rise from the combustor, in order to better predict and prevent unstart, and offer insight for engine control.

Shock trains exhibit complicated dynamics even when the boundary conditions are held nominally constant. The shock train position is inherently unsteady and the position fluctuations become more significant as the inflow Mach number is increased. Previous studies at higher Mach numbers have shown that the position fluctuations can be over a tunnel height away from the average location.[5–7] In addition, the movement of the shock train is coupled with pressure oscillations, which may generate detrimental noise or fluctuating wall loads. The mechanism behind these fluctuations is still unknown. Some theorized sources include turbulent fluctuations in the incoming flow,[8] upstream propagating disturbances from the diffuser,[9] fluctuations in boundary layer thickness,[10] and the unsteadiness resulting from the interaction with the boundary layer within the shock train itself.[10] A similar large-scale, low-frequency unsteadiness has been observed in many single SBLI experiments but the source of the unsteadiness is still open to debate.[11,12] However, for the shock train, the multiple separation regions can interact in complex ways. The dynamics we observe at steady-state may contribute to the motion of the shock train when a downstream forcing is applied.

The majority of computational studies only consider steady-state shock trains because most solvers use time-averaged physics and the addition of time-dependency greatly increases the complexity and cost of the analysis. Nonetheless, Hoeger et. al have used a 2-D transient computational model with back pressure as a time-dependent input to predict the location of a normal shock train in a Mach 1.8 inflow.[13] They found that when a large instantaneous back pressure is applied, the shock train first propagates upstream (against the incoming flow) with speeds up to 300 m/s. The shock train overshoots and then travels back downstream to its final rest position at up to 20 m/s. Decreasing the magnitude of the back pressure change reduces the shock train's speed and the amount of overshoot. In comparison, when the back pressure change is applied more gradually (at 8,500 kPa/s) the computational model predicts a maximum speed of 110 m/s as the shock rain travels monotonically upstream to the same rest location with no overshoot. The final location of the shock train agreed well schlieren images from an experimental setup where the back pressure was controlled by a downstream ramp (with a non-linear change in back pressure of about 50 kPa over 0.036 seconds).

Experimentally, downstream forcing has been applied primarily to determine optimal methods for detecting the shock train leading edge using wall pressure measurements.[14–16] This information can be used to develop active control methods or determine the effectiveness of passive methods. Such studies on stabilizing and controlling the shock train position have used devices including suction slots,[17] vortex generators,[18] and mass injection.[19] In these cases the back pressure steadily increases and the flow remains started.

Another way of examining the effects of downstream forcing is by increasing the back pressure until

inlet unstart occurs. Wagner et al.[2] initiate unstart in their experiment by deflecting a downstream flap. An interesting result they found is that the unstart process is seemingly independent of the flap deflection speed. The generated shock train was initially pushed upstream at roughly 26 m/s by the severe boundary layer separation from the flap body. Further upstream movement through the isolator was seen to be highly associated with separation induced by the shock system originating from the inlet. For this reason, other inlet-isolator models have shown a different progression of the shock train during unstart because of differences in geometry.[3,4,20] Similar results have been obtained with unstart was induced by mass addition.[21]

The goal of the current paper is to determine the details of how the shock train reacts to forcing introduced by a fluctuating back pressure. We want to understand how the following aspects impact the dynamics of the shock train: boundary layer thickness, magnitude of back pressure change, and the rate of change of back pressure. These parameters are different ways of modeling simple pressure disturbances that could be generated by a combustor. Ultimately, we want to better understand how the shock train responds to disturbances such that we can better predict, prevent and control unstart. Shock trains are complex systems, so the experiments described in this paper are designed to simplify the problem in order to better identify the underlying physics.

II. Experimental Setup

The current experiments are performed in a suction type wind tunnel at the University of Michigan.[5,22–24] A schematic diagram of the wind tunnel with relevant instrumentation is shown in figure 1. Air enters the wind tunnel intake and then conditioned by a flow conditioning section. The supersonic flow is generated by a one-sided converging-diverging nozzle that produces a nominal freestream Mach number of 2.0 and a unit Reynolds number of 1.4×10^7/m.

The test section has a constant-area, rectangular cross-section measuring 57.2 mm × 69.8 mm (width × height). Location ⓐ in figure 1 marks the start of the constant area cross-section and is the position where the inflow conditions are defined and measured. A summary of the inflow conditions is presented in table 1. Finally, a right-handed coordinate system is used for this work. The x-direction is oriented streamwise with $x = 0$ at the throat. The z-direction is normal to the bottom-wall. The origin is located on the lower right corner of the duct cross-section as one looks downstream.

A shock train is produced by partially closing a butterfly control valve (VAT series 612) separating the diffuser from the vacuum chamber. The reduced area for airflow increases the back pressure and a shock structure forms in the test section to match the pressure increase. The back pressure, p_b, is measured just upstream of the diffuser using a MKS 626C Baratron capacitance manometer (see location ⓑ in figure 1). The accuracy of the manometer is 0.25% of the reading and the response time is about 0.2 ms. Downstream forcing is introduced by periodically changing the valve angle and thus changing the back pressure. For the conditions of this experiment, the resulting shock train transitions from a normal shock train at higher back pressures (i.e., for longer shock trains) to an oblique shock train at lower back pressures (i.e., for short shock trains).[5]

In this paper we consider five cases of forcing. In all of the cases, a shock train is first stabilized in the test section by partially closing the control valve to an initial angle Θ_1. Then, a change in back pressure is

Nominal Mach number	2.0
Flow speed, m/s	517
Unit Reynolds number, m^{-1}	1.4×10^7
Stagnation pressure, kPa	99.7
Stagnation temperature, K	294
Static pressure, kPa	11.91
Static temperature, K	160
Density, kg/m^3	0.28
Viscosity, N-s/m^2	1.11×10^{-5}

Table 1. Summary of test section free stream inflow conditions.

generated by further closing the valve at a constant rate $\dot{\Theta}$ to a temporary angle Θ_2, waiting for a designated time Δt, and then opening the valve back to the initial position Θ_1 for a time Δt. This opening/closing process is repeated at a frequency Ω for several cycles over a total testing time of duration of about 2.75 seconds. In response to the cyclic operation of the control valve, the leading shock in the shock train oscillates between two positions in the test section. Note that the shock train is longer while at the upstream location (higher back pressure). This process is shown schematically in figure 2.

For all cases considered in the study, the rate of change of the control valve angle is maintained to the same value of $\dot{\Theta} = 300^\circ$ s^{-1}, while the forcing frequency Ω is increased from about 0.5 Hz to 3.5 Hz. Table 2 summarizes the different cases considered in the study. The cases are distinguished by a letter A - E. Because the total test time was nearly the same for all cases (approximately 2.75 seconds), cases A-E have an increasing number of cycles with the same initial and final valve angles. Quantitative analysis of the resulting back pressure time history forcing the shock train will be reported in the discussion section below.

Case	A	B	C	D	E
Θ_1, deg.	63.00	63.00	63.00	63.00	63.00
Θ_2, deg.	62.37	62.37	62.37	62.37	62.37
Δt, s	0.85	0.40	0.24	0.18	0.14
Ω, Hz	0.59	1.25	2.08	2.78	3.57

Table 2. Test conditions.

Schlieren imaging is used to track the location of the leading shock in the shock train and determine its speed. Borosilicate glass side-walls provide optical access along the full length of the wind tunnel. A folded z-type schlieren setup with a horizontal knife-edge was used to capture vertical gradients in the flow. The light source was fabricated in-house and uses a Luminus SBR-70 LED for continuous illumination.

Schlieren images are recorded with a Phantom v711 camera at a rate of 25 kHz with an exposure time of 1 μs. The image resolution is about 3.9 pixel/mm. The camera's spatial resolution limitations restrict the field of view to a portion of the full shock train system. Figure 3 shows a representative schlieren image of the instantaneous shock train system generated with a constant back pressure.[5,25] The indicated inset describes the relative size of the imaging region used in these experiments. The region captures the center portion of the duct, about $\pm$20 mm around the duct midplane, with a total length of 130 mm.

The individual instantaneous schlieren snapshots are processed using a shock detection algorithm to automatically detect the streamwise position of the Mach stem triple point of the leading shock in the system. We define this position x_I, following the convention set in our previous work.[5,25] Thus, we are able to obtain temporal data of the leading shock streamwise position sampled at 25 kHz. An 11-point Gaussian filter with a $1/e$ full-width size of 85 μs is used to smooth the data prior to data analysis.

III. Results

A. Description of the shock train forcing scheme

The method of forcing described in the previous section creates a pressure disruption which interacts with two systems. The change in valve angle sends pressure waves upstream through the diffuser which ultimately effects the shock train. Thus, the diffuser and test section systems are impacted by the valve angle and have coupled responses. Within the test section we measure two responses: the back pressure measured at the end of the test section (point Ⓓ) and the shock location at the beginning of the system (measured location x_I). As an example, we will discuss figure 4 which compares the time traces of valve angle, shock position, and back pressure for case A (the lowest forcing frequency case). In this case, there are three distinct regions of time where all of the signals are nominally constant and the system is at rest: $t < 0.85$, $1.15 < t < 1.70$, and $2.00 < t < 2.55$ seconds.

For $t < 0.85$ the valve angle is at $\Theta = \Theta_1$ and the shock system is located at a downstream rest position. The shock position is nominally constant but small fluctuations are evident in the time trace due to an inherent unsteadiness in the shock train system. Our previous studies[5] with this experimental setup have shown that with a nominally constant back pressure the position fluctuations can reach up to 25 mm away from the mean position. However, 98% of the position fluctuations are within 9.5 mm of the average

location. Similarly, the back pressure is not a constant value while the system is at rest because the shock train generates turbulence and pressure fluctuations that are read by the manometer. These small back pressure fluctuations become more prominent when the shock train is located further downstream, closer to the back pressure measurement point. An example instantaneous schlieren snapshot taken during this period of time is shown in figure 6(a). Only the leading shock is within the field of view. The Mach stem can be clearly identified between two large lambda feet allowing the x-location of the triple point (marked as x_I in the figure) to be found.

At $t = 0.85$ in figure 4 the valve angle changes and downstream pressure disturbances push the shock train to a new location. As expected, the valve angle is positively correlated with shock position and negatively correlated with back pressure. Thus, a decrease in valve angle (valve is more closed) leads to a decrease in position (shock train moves upstream) and increase in back pressure. Notice that as the leading shock transitions to an upstream position the time trace still contains small fluctuations due to the system's inherent unsteadiness. This high-frequency component is superimposed onto the bulk motion of the shock train. Therefore, there are some instances in time when the shock train momentarily travels downstream during the transition process to an upstream rest position. However, there is no evidence of overshoot as the shock train reaches its next rest position. Thus, once the leading shock reaches its average rest position the only variation in position is due to the system's inherent unsteadiness. Figure 6(b) is an example schlieren snapshot of the shock train progressing through the field of view. Flow is from left to right, while the shock train propagates from right to left.

Consider a small portion of the time trace in figure 5. This zoomed in section shows a clear time delay between the change in valve angle and response of the shock train system. For the first transition of case A (shown in the figure) the time delay of the shock position (τ_x) is 20 ms and the time delay of the back pressure (τ_p) is 37 ms. This indicates that the upstream part of the shock train responds before the downstream section. While we discuss the upstream shock position and downstream back pressure responses separately it is important to remember that the shock train is a highly interconnected system and may react to the changing valve angle in a complex manner. We will discuss this further in section B.

In addition, figure 5 demonstrates that shock train is sensitive to the valve angle and responds slowly to forcing. The relative change in valve angle is substantially smaller than the resulting change in back pressure and shock position. Less than a 1 degree change in valve angle leads to a large change of 3 kPa in back pressure and an 80 mm movement of the leading shock. Since the change in valve angle is very small, the transition occurs in less than 2.1 ms at the constant rate of $\dot{\Theta} = 300^{\circ}\text{s}^{-1}$. The time scale over which the system responds is substantially longer. For case A, the rise time for the shock position (T_x) and back pressure (T_p) are approximately 200 and 300 ms, respectively.

Return to the full time trace in figure 4. When $1.15 < t < 1.70$ the valve angle is at $\Theta = \Theta_2$ and the shock system is at rest, located at a upstream position. Our previous work has shown that the fluctuation component due to the shock train's inherent unsteadiness is statistically the same at the upstream location as the original downstream location.[5] An example schlieren snapshot of the shock train during this region of time can be seen in figure 6(c). Notice that the shock train has become longer and thus the second shock in the system is now visible within the schlieren field of view. Finally, the transition process repeats in reverse to complete the cycle. The valve angle returns to $\Theta = \Theta_1$ and the shock train position and back pressure adjust to match the new downstream boundary condition.

We gain additional insight on the system by examining the shock train speed. The speed of the leading shock in the shock train, u_I, is calculated from the time-history measurement of the shock position as the central difference of between positions. The time trace of the shock speed for case A is shown in figure 7(a). The shock train position can fluctuate with speeds up to 15 m/s due to the inherent unsteadiness of the system. Contrary to the shock position, the time trace of shock speed does not reveal a clear oscillatory behavior that would be expected as a result of the forcing. Thus, the magnitude of the high-frequency speed fluctuation component must be higher than the bulk propagation speed of the shock train during the cyclic forcing. In other words the response of the shock train is slower than the fluctuations due to inherent unsteadiness. To emphasize the different frequency components, we decompose the shock propagation speed as:

$$u_I(t) = U_I(t) + u'_I(t)$$

where U_I and u'_I are the bulk (low frequency) and fluctuation (high frequency) components, respectively. In practice, the bulk propagation speed is found by low-pass filtering the original data with a cutoff frequency of 50 Hz. The time trace of the bulk propagation speed for case A is shown in figure 7(b). As the shock train

moves upstream and downstream the subsequent bulk shock speeds are negative and positive, respectively.

Another potentially important variable is the rate of change in back pressure. During the transition periods in all of the cases there is a continuous smooth variation in back pressure at a variable rate ($\mathrm{d}p_b/\mathrm{d}t$). We compute this value from the time-history measurement of the back pressure as the central difference between values. An example time trace for case A is shown in figure 8. The back pressure rate of change is positive and then negative for the upstream and downstream movements, respectively. The maximum rate of change of p_b occurs roughly midway in the back pressure transition.

Thus far we have only considered the responses to a change in valve angle for case A. The higher forcing frequency cases show similar trends and will be discussed more thoroughly in the next section.

B. Effects of forcing frequency on shock train response

Given this underlying knowledge of the shock train responses to the changing valve angle we now consider the effects of increasing forcing frequency while maintaining the same initial and final valve angles. Figures 9(a) and 9(b) show the back pressure and leading shock position time traces, respectively, for all of the cases. Both variables are normalized by their respective average values at the rest point before any downstream pressure forcing, $p_b^\star$ and $x_I^\star$. The starred quantities are calculated by taking the average of the value between $0 < t < \Delta t$. As expected from the discussion above, the back pressure increases and the shock location decreases (i.e., it moves upstream to a smaller x) with decreasing valve angle.

On closer inspection of figure 9, we find that the oscillation frequency of back pressure and leading shock position match the forcing frequency for all of the cases. However, as forcing frequency is increased the back pressure and shock position time histories never reach a stationary value over the period, unlike the valve angle time history. Thus, the response signals more closely resemble a sine wave at higher forcing frequencies. Especially evident in figure 9(a), is a difference in back pressure between the beginning and end of the first cycle even though the valve angles are the same. After this initial yield in back pressure the extrema values are approximately constant from cycle to cycle. Thus, there is a back pressure yield within the first cycle and then a limit cycle is reached.

As a first method of comparing different cases of forcing frequency, we define the maximum and minimum back pressures for each individual case as p_b^+ and p_b^-, respectively. These are calculated by averaging extrema values across all of the limit cycles for a given case. Figure 10(a) shows the maximum (p_b^+) and minimum (p_b^-) back pressure values normalized by $p_b^\star$ for case C on the back pressure time trace. Note that p_b^- is noticeably higher than $p_b^\star$.

In a similar fashion, we define the maximum and minimum shock position for each case as x_I^+ and x_I^-, respectively. Figure 10(b) shows the maximum (x_I^+) and minimum (x_I^-) values normalized by $x_I^\star$ for case C on the time trace of leading shock position. While there was a drastic yield in back pressure, figure 10(b) does not show much difference between $x_I^\star$ and x_I^+. Thus, in all the cycles the leading shock oscillates between the same two positions.

Figures 11(a) and 11(b) compare the maximum and minimum values for back pressure and leading shock position, respectively, for the different cases of forcing frequency. As forcing frequency increases the maximum achieved back pressure decreases and the minimum achieved back pressure increases. In other words, the overall change in back pressure during the cycle is reduced. From case A to case E the change in back pressure of a cycle is reduced by approximately 60%. Figure 11(b) shows a similar trend in the average values of x_I^+ and x_I^-. Increasing the forcing frequency decreases x_I^+ and increases x_I^- such that the shock train travels less distance. the shock train in case E travels 30% less distance than the shock train in case A. At this point we cannot determine if this reduction in shock train motion is due to a slow response time of the shock train relative to the forcing frequency or the resulting reduction of back pressure change.

Finally, we repeat the above analysis for the time rate of change of back pressure and bulk speed of the leading shock (i.e. the first derivatives of the variables considered above). Figure 12(a) shows how the maximum ($[dp_b/dt]^+$) and minimum ($[dp_b/dt]^-$) rates of change in back pressure change with forcing frequency. There is only a 20% reduction in the maximum back pressure rate of change from case A to E. A slightly larger reduction of 30% is evident in the magnitude of the minimum rate of change from case A to E. For a given case the magnitudes of extrema are approximately the same. The average rate of change across all of the cases is 15 kPa/s and the extrema in the rate of change occurs roughly midway in the transition.

Next, consider the plot of maximum (U_I^+) and minimum (U_I^-) bulk speed versus forcing frequency in figure 12(b). Unlike the other variables, the extrema in bulk speed appears to be independent of forcing frequency. The average value of U_I^+ across all cases is 0.80 m/s while the average value of U_I^- is only -0.67

m/s. The difference in magnitudes indicates that the shock train propagates faster when moving downstream, i.e. in the direction of the bulk fluid flow.

As discussed in the previous section there is a time delay between the valve angle changing and the response of the system. We compute the time delay for each cycle by identifying the point at which the signal's derivative is 20% of its extrema value. For example, the time delay of the leading shock position is defined as the time difference between the change in valve angle and the time at which the bulk speed reaches 20% of the maximum or minimum value for the cycle (approximately 0.15 m/s). Analogously, the time delay for back pressure occurs when dp_b/dt reaches 20% of the maximum/minimum (approximately 3 kPa/s).

The average time delay across all of the cycles is plotted versus the forcing frequency of each case in figure 13(a). The delay of the leading shock (τ_x) is in blue and the delay of the back pressure (τ_p) is in red. The error bars are due to the slow sampling rate (p_b is measured at 50 Hz and x_I is low pass filtered at 50 Hz to compute the bulk speed). There is a slight increase in delay time of the leading shock with increased forcing frequency. However, this result is unclear given the potential errors. A stronger trend of increasing time delay with increased forcing frequency is evident in the curve for back pressure. In all of the cases the time delay of back pressure is larger than the delay of leading shock position. Thus, the upstream response of the shock train occurs before the downstream response.

We have already found the first point in a cycle where the signal's derivative is 20% of the maximum/minimum. The rise time is the time between this point and the next point at which the derivative is 20% of the extrema value and the second derivative has the opposite sign. Figure 13(b) shows how the rise time of the leading shock (blue curve) and back pressure (red curve) change with forcing frequency. Once again, the error bars are due to the 50 Hz sampling rate of the derivatives (U_I and dp_b/dt). The back pressure clearly has a longer rise time than the leading shock position at low forcing frequencies. However, the difference between T_x and T_p decreases at higher Ω. The black, dashed line represents half of the cycle time for a given Ω. As forcing frequency increases the rise times decrease and approach the dashed curve. Thus, higher forcing frequencies limit the time during which the system can respond. At lower forcing frequencies the rise times diverge from the dashed line. In addition, there is more variation in rise time of different cycles for lower frequency cases. For example, some cycles in case B show a quick initial response (where the derivative of the signal is high) but then slow down at the end of the transition and gradually reach the final resting point. Thus, the rise times are consistently defined but potentially underestimate the true rise time of the signal at lower forcing frequencies.

C. Shock train trajectory

In the previous section we saw a yield in the back pressure during the first cycle despite returning the valve to the same angle. To better differentiate between the affects of changing back pressure and forcing frequency, we have compiled the trajectory of the leading shock of the shock train as the back pressure oscillates.

Figure 14(a) is a plot of the normalized location of the leading shock versus normalized back pressure for case A. At the beginning of the cycle $p_b \simeq p_b^\star$ and $x_I \simeq x_I^\star$. The downstream forcing from the change in valve angle causes the shock train to travel in a counter-clockwise loop. There is a clear hysteresis effect during the cyclic motion that causes the shock train to travel along different paths during the upstream and downstream moving portion of the cycle. Also note that the leading shock system does not monotonically travel upstream, but instead a fluctuation component is superimposed to the bulk component. The superimposed fluctuation is qualitatively similar to that observed in the quasi-steady state studies where the shock fluctuated about a mean position at a given constant back pressure.[5]

The shock train trajectory for case C is shown in figure 14(b). Case C has multiple cycles and each cycle is marked by a different color. The back pressure yield is clearly evident because the first cycle starts at a different location than the remaining cycles. However, within the limit cycle there are only minor differences between the motion of the shock train from cycle to cycle, which are due to the instantaneous shock position fluctuations superimposed on to the bulk motion of the shock. Thus, within the limit cycle the back pressure and shock train position follow a consistent path. The same is true for the other cases with multiple cycles.

In figure 15 the trajectories of the leading shock during the first and second cycles are compared across all of the cases. Notice that in the first cycle (figure 15(a)) the shock train position does not make a closed loop because the back pressure does not recover to its initial value. The cycle plotted in figure 15(b) is a closed loop because the back pressure and shock position recover to approximately the same values at the

beginning of the cycle. Also notice that the loop becomes smaller with increased forcing frequency because of the increased yield in back pressure and subsequent drop in distance traveled by the leading shock.

Since the yield in back pressure increases with forcing frequency we re-normalize the plots to better compare the trajectory of different cases. In figure 16 the shock position and back pressure are normalized by the maximum and minimum values of the case (see section B). Therefore, a value of zero signifies that the variable is equal to its minimum value, while a value of one signifies the variable is equal to its maximum value. Figures 16(a) and 16(b) show the normalized shock trajectories for the first and second cycle, respectively, for all of the cases. The normalized shock trajectories for different cases now follow a similar path. In the first cycle the major differences between cases occurs before the limit cycle is reached. The remaining differences between cases and cycles appear to be due to the small fluctuation component superimposed to the bulk shock motion. This result indicates that, within the limited forcing frequency range of the current study, the shock train trajectory is independent of the forcing frequency and simply depends on the history of the back pressure.

The average shock train trajectory in the limit cycle is computed by averaging the overlapping trajectories for all of the cases and for all of the cycles after the first loop. The solid, black line in figure 17 is the resulting average curve. We note that the average trajectory closely follows the path of a fifth order polynomial. For the upstream movement of the shock train the polynomial fit is:

$$\frac{x_I - x_I^-}{x_I^+ - x_I^-} = -4.06P^5 + 13.03P^4 - 15.62P^3 + 9.11P^2 - 3.21P + 0.85$$

where P is the normalized back pressure value $P = (p_b - p_b^-)/(p_b^+ - p_b^-)$. In a similar manner, the polynomial fit for the downstream motion of the shock train is:

$$\frac{x_I - x_I^-}{x_I^+ - x_I^-} = -5.64P^5 + 9.97P^4 - 5.33P^3 + 0.11P^2 + 0.18P + 0.89$$

The collapsed normalized trajectory indicates that the path of the shock train is independent of forcing frequency and instead depends on the history of the back pressure.

The trajectory of the shock train can also be studied using the derivatives of the measured responses. Figures 18(a)–(c) are plots of the bulk speed versus the time rate of change of back pressure for cases A, C, and E, respectively. There are clear differences in the shock speed cycle as forcing frequency is increased.

In figure 18(a) the single cycle for case A is plotted. The cycle begins at (0, 0), which is a rest position where the shock speed and back pressure derivatives are close to zero. The scatter between these points is due to the inherent unsteadiness of the system. Following the change in valve angle, the back pressure rate increases and the speed of the shock rapidly increases in the negative direction (i.e. moves upstream). Arrows 1 and 2 in the figure mark the counter-clockwise loop in the trajectory that occurs after the first change in valve angle. The peak negative speed is reached when the back pressure rate of change is about 15 kPa/s. Then, the speed decreases as the shock train gradually moves upstream until the next rest position. At the upstream rest position the trajectory has again stabilized at the point (0, 0). When the valve angle changes for a second time, the shock train responds by traveling a similar, counterclockwise path (see arrows 3 and 4) in the other quadrant of the figure, thus forming a tilted figure-eight pattern. In this case, the shock train returns to its rest position after every change in valve angle.

The effects of increased forcing frequency start to become evident in figure 18(b). In case C, the direction of the speed's loop is the same (counter-clockwise) but the center of the figure-eight is less defined. There are less points at the rest locations because the shock train is oscillating faster. Finally, in case E (figure 18(c)) the speed cycle now looks like a circle instead of a figure-eight. The points at (0, 0) occur before any back pressure forcing ($t < \Delta t$). Following the numbered arrows, the trajectory makes a counter-clockwise loop without ever returning to the point (0, 0). This means that the leading shock changes direction (i.e. the trajectory crosses the x-axis) before the limiting value of back pressure is achieved (i.e. the trajectory crosses the y-axis). Thus, in this case the shock train is never truly at rest when there is downstream forcing introduced by the valve. Cases B and D were not plotted but there is a clear transition between cases with rest points and cases without rest points from case A - E (i.e. increasing forcing frequency). We conjecture that the changes in the speed cycle from case to case are due to the limits in the temporal response of the shock train system.

IV. Conclusions

The properties of an oscillating shock train due to downstream pressure forcing are studied. Forcing is introduced by changing the angle of a downstream control valve. In response, the shock train is pushed to a new location in the duct, effectively changing the length of the shock train and the downstream pressure (p_b) measured at the end of the duct. Five cases of forcing are considered to observe the effects of increasing forcing frequency. These different cases are used to model different ways the back pressure could change in an actual combustor, thus inducing shock train propagation in the isolator. Some of the key results are as follows:

1. Within the first cycle of the response there is a yield in back pressure (i.e. the back pressure does not return to its original value even though the valve returns to its initial angle). After this yield a limit cycle is reached and all remaining oscillations occur between the same back pressure values. Increasing forcing frequency will increase the amount of back pressure yield.

2. There is no yield in the leading shock position and thus, the shock train oscillates between the same two points throughout all of the cycles. However, the shock train travels less distance due to the decrease in back pressure change at higher forcing frequencies.

3. The shock train's bulk speed (generally less than 1 m/s) is less than the speed of the high-frequency fluctuation component (up to 15 m/s). The bulk speed extrema values are independent of forcing frequency. However, the leading shock tends to travel faster in the downstream direction (with the bulk fluid flow).

4. The leading shock in the shock train responds to the valve's forcing before the back pressure. Thus, the upstream portion of the system responds first. There is a slight increase in the delay times with increased forcing frequency.

5. At low forcing frequencies the back pressure has a longer rise time than the leading shock position's response. The response times approach half of a cycle time at higher forcing frequencies meaning the response of the system is limited by the downstream forcing.

6. There is a hysteresis effect during the shock train's cyclic motion that causes the leading shock to travel along different paths during the upstream and downstream moving portion of the cycle. When normalized by the maximum and minimum back pressures and shock positions of the limit cycle all of the cases follow the same trajectory. Deviations from this average path are due to the shock train's high-frequency fluctuation component. A collapsed trajectory for all cases of forcing frequency indicates that the motion of the leading shock is determined by the history of the back pressure.

References

[1]Matsuo, K., Miyazato, Y., and Kim, H., "Shock train and pseudo-shock phenomena in internal gas flows," *Progress in Aerospace Sciences*, Vol. 35, No. 1, 1999, pp. 33–100.

[2]Wagner, J. L., Yuceil, K. B., Valdivia, A., Clemens, N. T., and Dolling, D. S., "Experimental investigation of unstart in an inlet/isolator model in Mach 5 flow," *AIAA Journal*, Vol. 47, No. 6, jun 2009, pp. 1528–1542.

[3]Rodi, P. E., Emami, S., and Trexler, C. A., "Unsteady pressure behavior in a ramjet/scramjet inlet," *Journal of propulsion and power*, Vol. 12, No. 3, 1996.

[4]Tan, H., Li, L., Wen, Y., and Zhang, Q., "Experimental investigation of the unstart process of a generic hypersonic inlet," *AIAA Journal*, Vol. 49, No. 2, feb 2011, pp. 279–288.

[5]Klomparens, R. L., Gamba, M., and Driscoll, J. F., "Structure and unsteadiness characteristics of shock trains," *under preparation for AIAA Journal*, 2015.

[6]Sugiyama, H., Tsujiguchi, Y., and Honma, T., "Structure and oscillation phenomena of pseudo-shock waves in a straight square duct at mach 2 and 4," *15th AIAA International Space Planes and Hypersonic Systems and Technologies Conference, AIAA paper 2008-2646*, American Institute of Aeronautics and Astronautics, apr 2008.

[7]Lindstrom, C. D., Davis, D., Williams, S., and Tam, C., "Shock-train structure resolved with absorption spectroscopy part II: analysis and CFD comparison," *AIAA Journal*, Vol. 47, No. 10, oct 2009, pp. 2379–2390.

[8]Ikui, T., Matsuo, K., Nagai, M., and Honjo, M., "Oscillation phenomena of pseudo-shock waves," *Bulletin of JSME*, Vol. 17, No. 112, 1974, pp. 1278–1285.

[9]Yamane, R., Takahashi, M., and Saito, H., "Vibration of pseudo-shock in a straight duct," *Bulletin of JSME*, Vol. 27, No. 229, 1984, pp. 1393–1398.

[10]Sugiyama, H., Takeda, H., Zhang, J., Okuda, K., and Yamagishi, H., "Locations and oscillation phenomena of pseudo-shock waves in a straight rectangular duct," *The Japan Society of Mechanical Engineers International Journal*, Vol. 31, No. 1, 1988, pp. 9–15.

[11]Dolling, D. S., "Fifty years of shock-wave/boundary-layer interaction research - What next?" *AIAA Journal*, Vol. 39, No. 8, 2001, pp. 1517–1531.

[12]Clemens, N. T. and Narayanaswamy, V., "Low-frequency unsteadiness of shock wave/turbulent boundary layer interactions," *Annual Review of Fluid Mechanics*, Vol. 46, No. 1, jan 2014, pp. 469–492.

[13]Hoeger, T. C., King, P. I., Donbar, J. M., and Cox-Stouffer, S., "2-D transient CFD model of an isolator shock train," *17th AIAA International Space Planes and Hypersonic Systems and Technologies Conferen, AIAA paper 2011-2221*, 2011.

[14]Le, D. B., Goyne, C. P., and Krauss, R. H., "Shock train leading-edge detection in a dual-mode scramjet," *Journal of Propulsion and Power*, Vol. 24, No. 5, sep 2008, pp. 1035–1041.

[15]Hutzel, J. R., Decker, D. D., Cobb, R. G., King, P. I., Veth, M. J., and Donbar, J. M., "Scramjet isolator shock train location techniques," *49th AIAA Aerospace Sciences Meeting including the New Horizons Forum and Aerospace Exposition, AIAA paper 2011-402*, American Institute of Aeronautics and Astronautics, jan 2011.

[16]Sajben, M., Donovan, J. F., and Morris, M. J., "Experimental investigation of terminal shock sensors for mixed-compression inlets," *Journal of Propulsion and Power*, Vol. 8, No. 1, 1992, pp. 168–174.

[17]Weiss, A. and Olivier, H., *Influence of a normal slot boundary layer suction system onto a shock train*, Vol. 2, Springer Berlin Heidelberg, 2012.

[18]Valdivia, A., Yuceil, K. B., Wagner, J. L., Clemens, N. T., and Dolling, D. S., "Control of supersonic inlet-isolator unstart using active and passive vortex generators," *AIAA Journal*, Vol. 52, No. 6, jun 2014, pp. 1207–1218.

[19]Huang, H., Tan, H., Wang, J., Sun, S., and Ning, L., "A fluidic control method of shock train in hypersonic inlet/isolator," *50th AIAA/ASME/SAE/ASEE Joint Propulsion Conference, AIAA paper 2014-3846*, 2014, pp. 1–13.

[20]Geerts, J. S. and Yu, K. H., "Visualization of shock train-boundary layer interaction in Mach 2.5 isolator flow," *43rd AIAA Fluid Dynamics Conference, AIAA paper 2013-3102*, American Institute of Aeronautics and Astronautics, jun 2013.

[21]Do, H., Im, S., Mungal, M., and Cappelli, M., "The influence of boundary layers on supersonic inlet unstart," *17th AIAA International Space Planes and Hypersonic Systems and Technologies ConferenAIAA paper 2011-2349*, 2011.

[22]Lapsa, A. P. and Dahm, W. J. A., "Stereo particle image velocimetry of nonequilibrium turbulence relaxation in a supersonic boundary layer," *Experiments in Fluids*, Vol. 50, No. 1, jun 2010, pp. 89–108.

[23]Eagle, W. E. and Driscoll, J. F., "Shock waveboundary layer interactions in rectangular inlets: three-dimensional separation topology and critical points," *Journal of Fluid Mechanics*, Vol. 756, 2014, pp. 328–353.

[24]Morajkar, R. R., Driscoll, J. F., and Gamba, M., "Experimental study of supersonic turbulent corner flow evolution in a low aspect ratio rectangular channel," .

[25]Klomparens, R. L., Driscoll, J. F., and Gamba, M., "Unsteadiness characteristics and pressure distribution of an oblique shock train," *AIAA paper No. 2015-1519*, 2015.

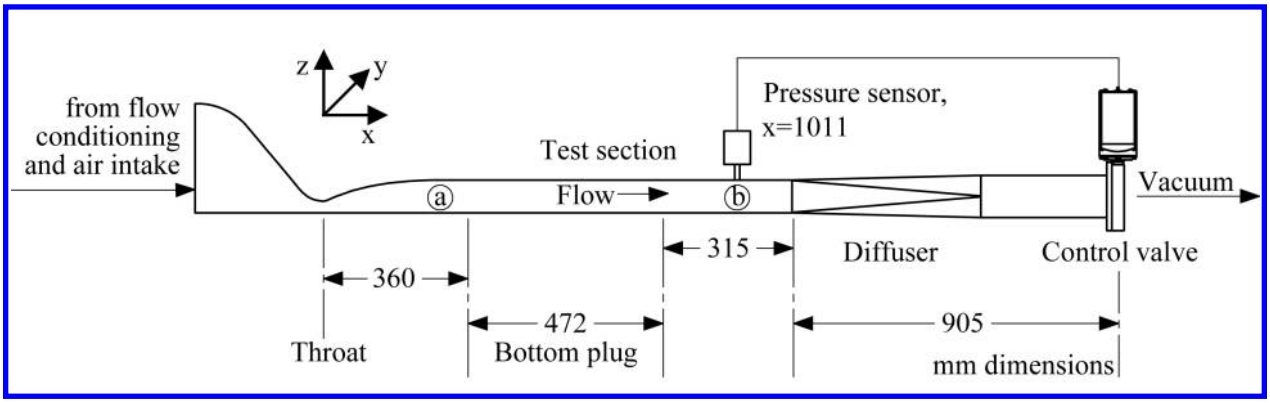

Figure 1. Schematic diagram of the wind tunnel.

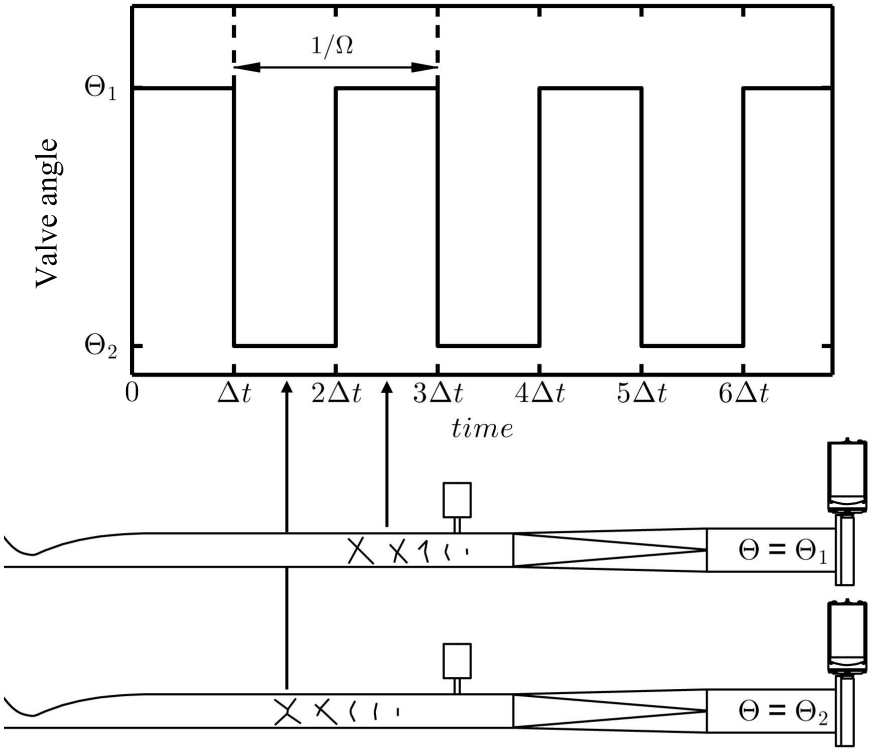

Figure 2. Schematic diagram of the shock train forcing scheme.

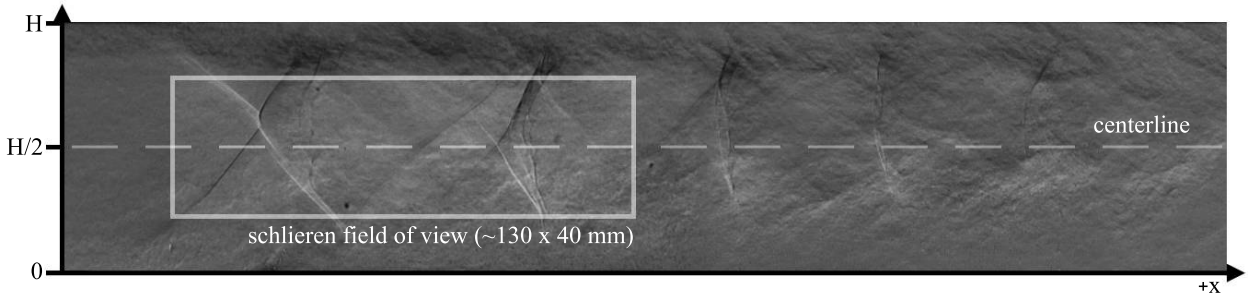

Figure 3. Image of a typical shock train with inset indicating the relative schlieren field of view.

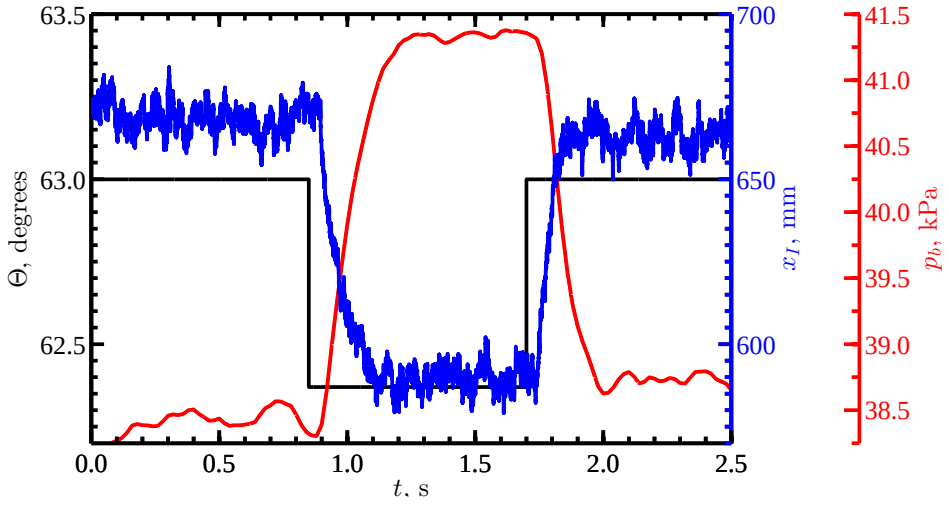

Figure 4. Valve angle (black line), back pressure (blue line), and leading shock position (red line) versus time for case A.

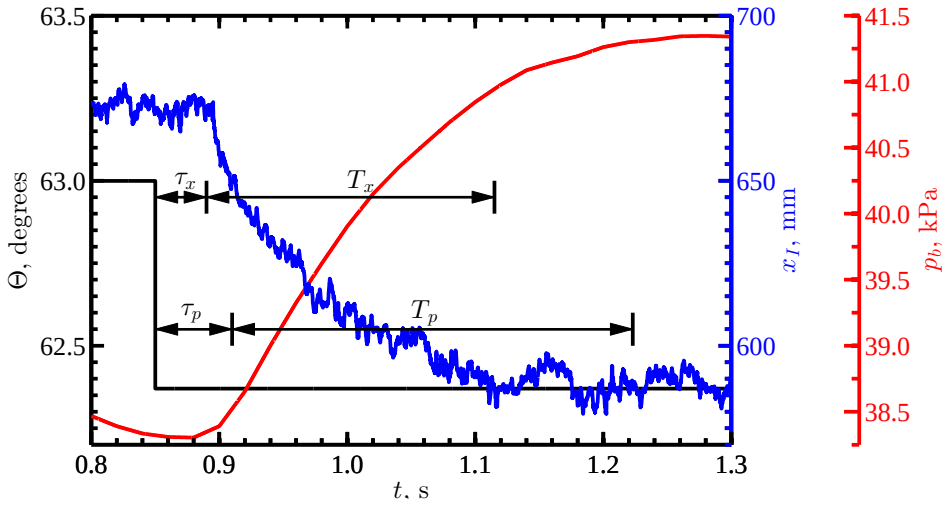

Figure 5. Valve angle (black line), back pressure (blue line), and leading shock position (red line) versus time for a portion of the run time of case A.

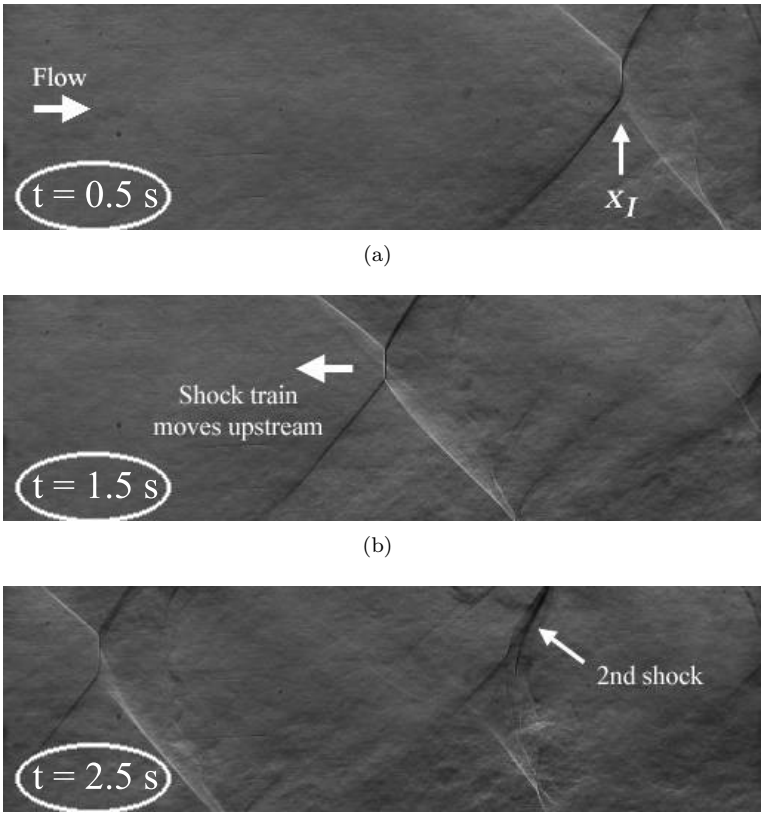

Figure 6. Instantaneous schlieren images: (a) downstream rest location $\Theta = \Theta_1$; (b) shock train moving upstream; (c) upstream rest location $\Theta = \Theta_2$.

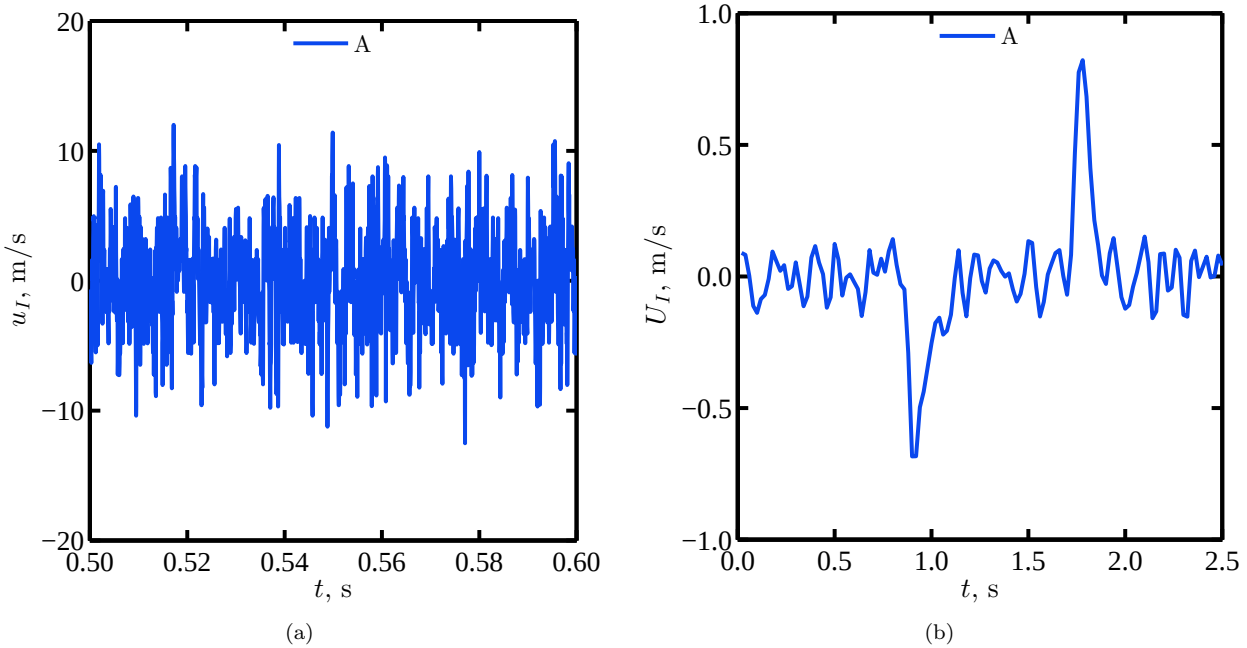

Figure 7. Time trace of speed components for case A: (a) total speed; and (b) bulk speed.

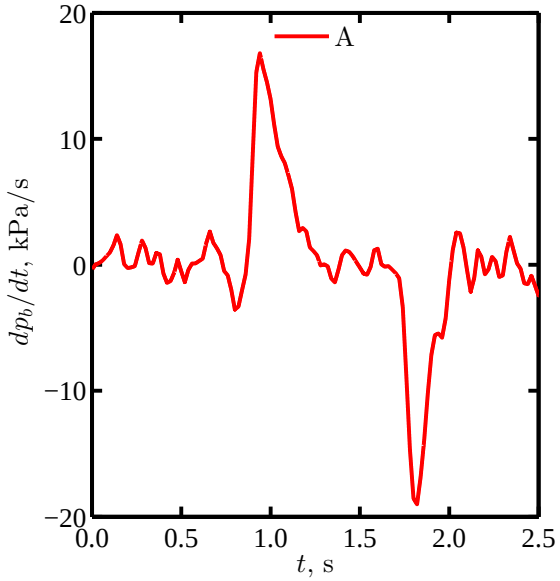

Figure 8. Time trace of the rate of change of back pressure for case A.

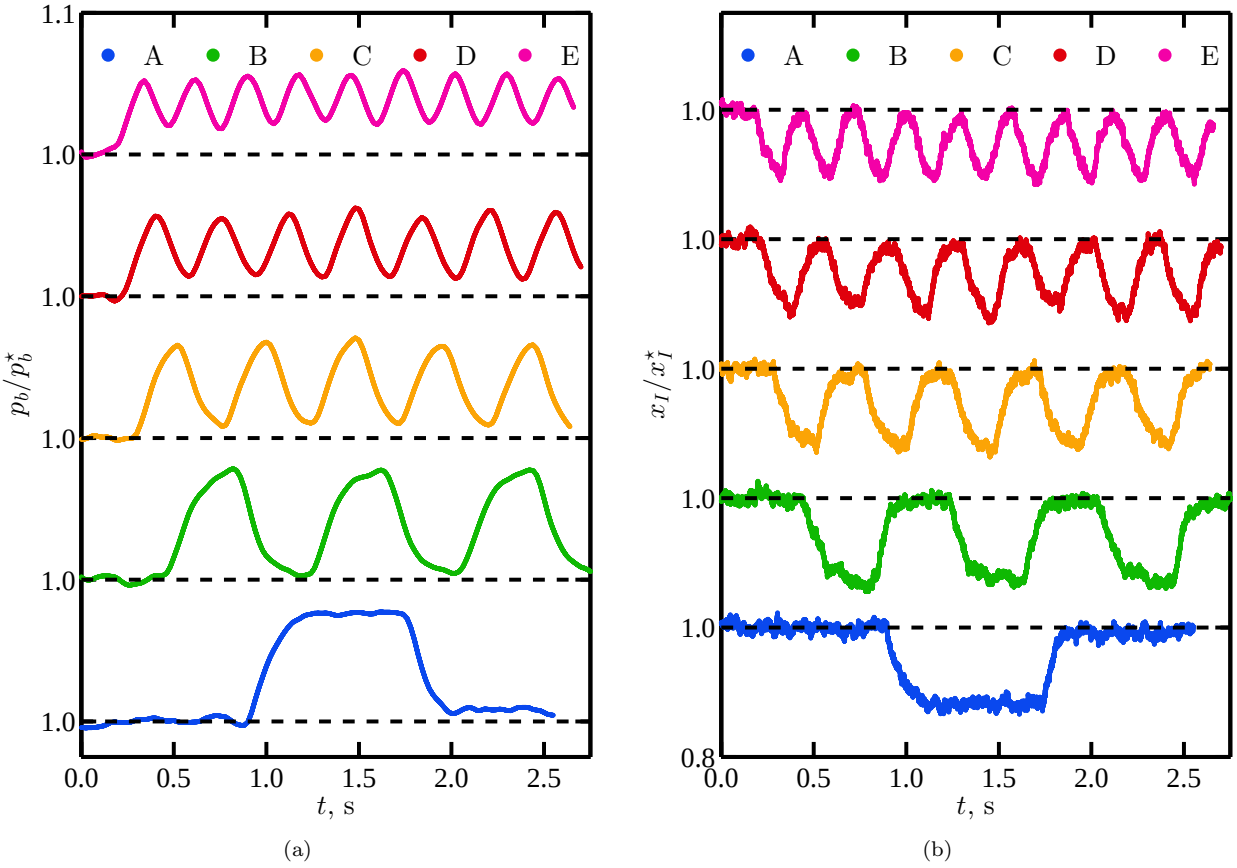

(a) (b)

Figure 9. Time traces of cases A-E: (a) back pressure; and (b) leading shock position.

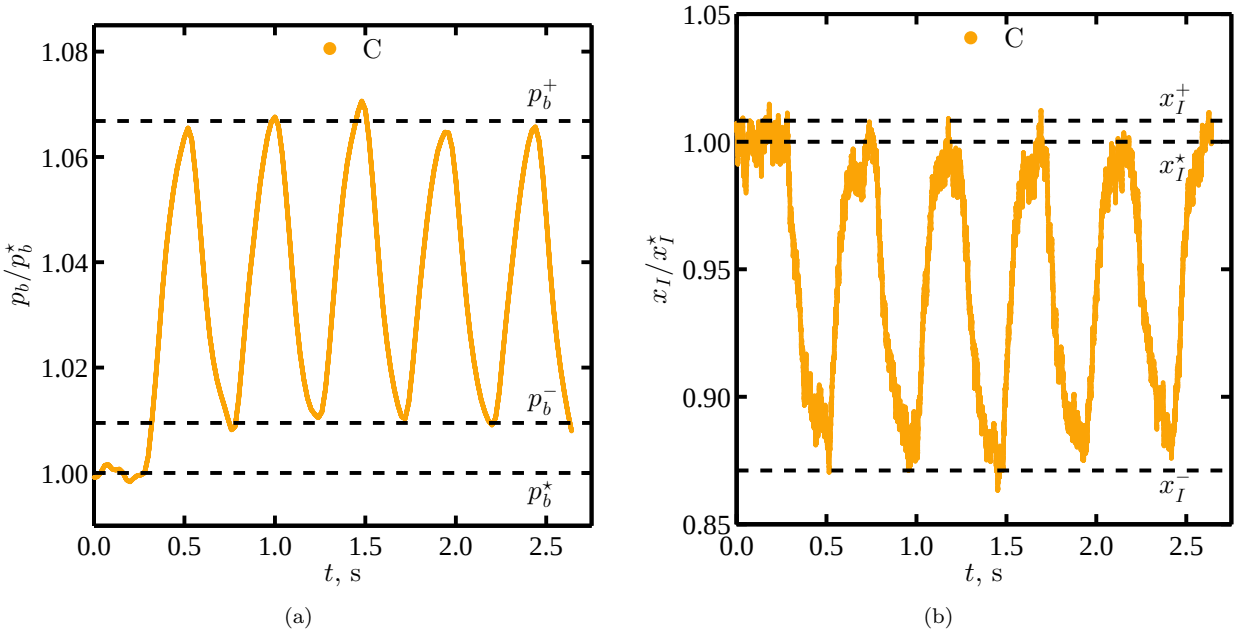

Figure 10. Case C time traces pointing out the maximum and minimum values calculated by averaging the extrema values across all of the cycles: (a) back pressure (b) leading shock position.

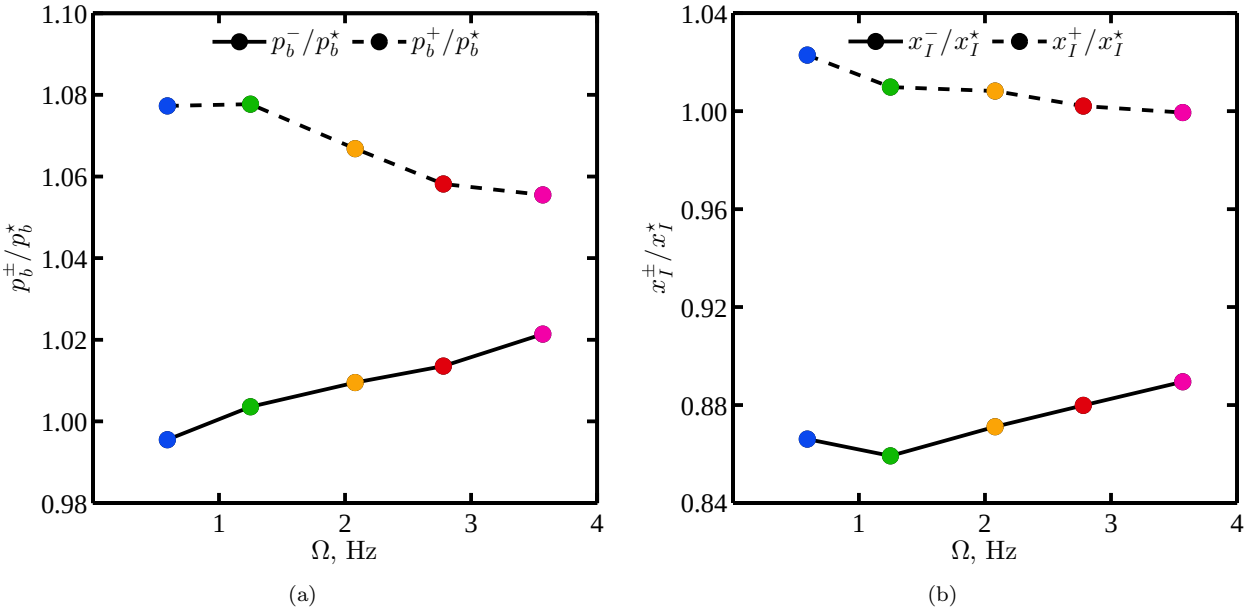

Figure 11. Normalized maximum and minimum values versus forcing frequency: (a) shock location; and (b) back pressure.

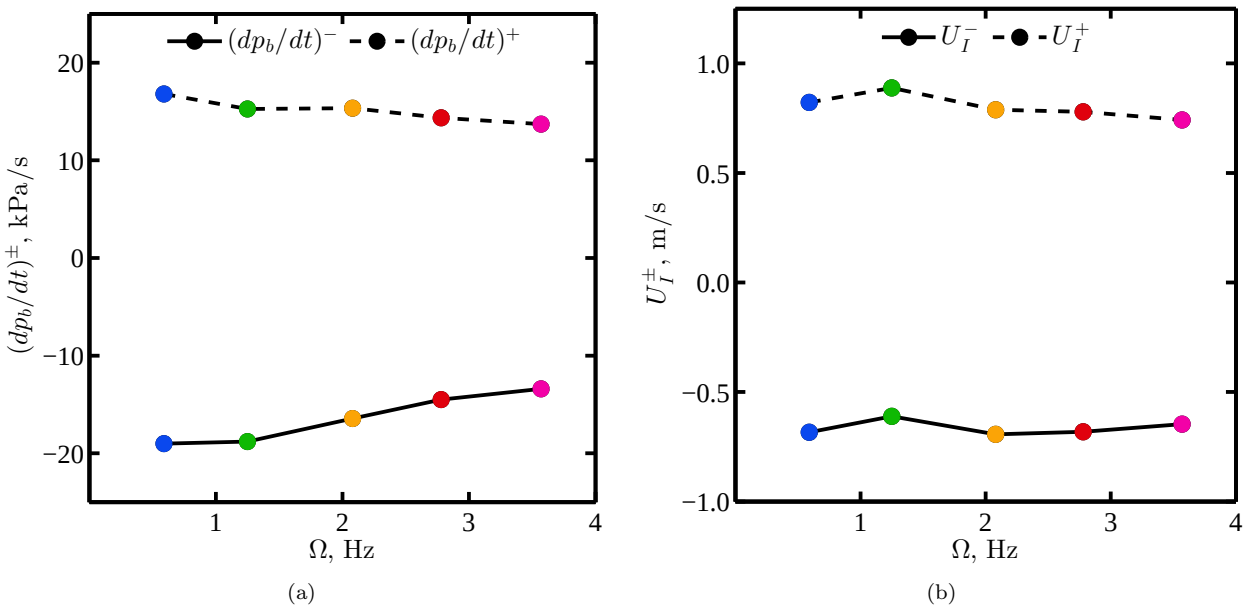

Figure 12. Maximum and minimum values versus forcing frequency: (a) rate of change of back pressure; and (b) shock speed.

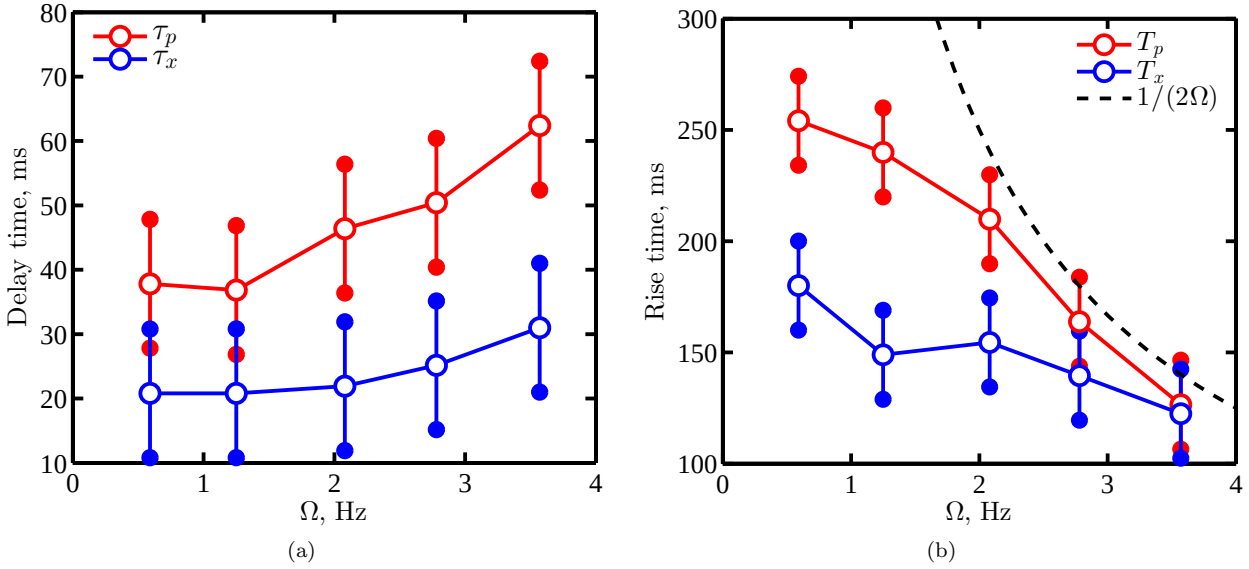

Figure 13. Comparison of cases A-E: (a) delay times; and (b) rise times.

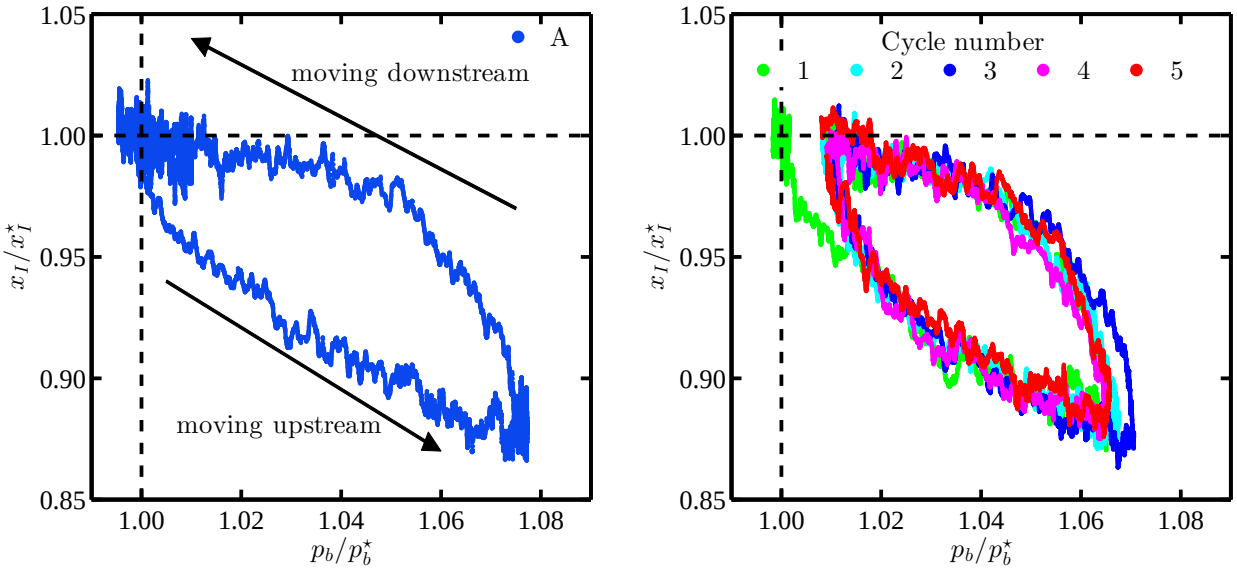

Figure 14. Normalized shock position versus normalized back pressure to demonstrate hysteresis: (a) case A; and (b) case C.

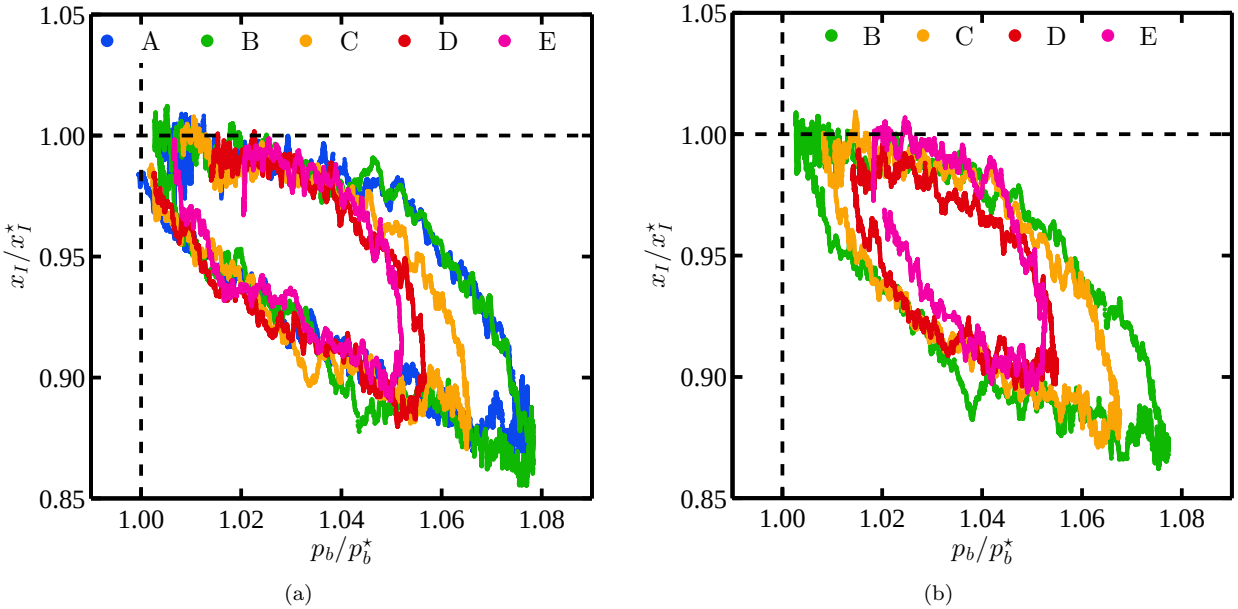

Figure 15. Plots of normalized shock position versus normalized back pressure for cases A-E: (a) the first cycle; and (b) the second cycle.

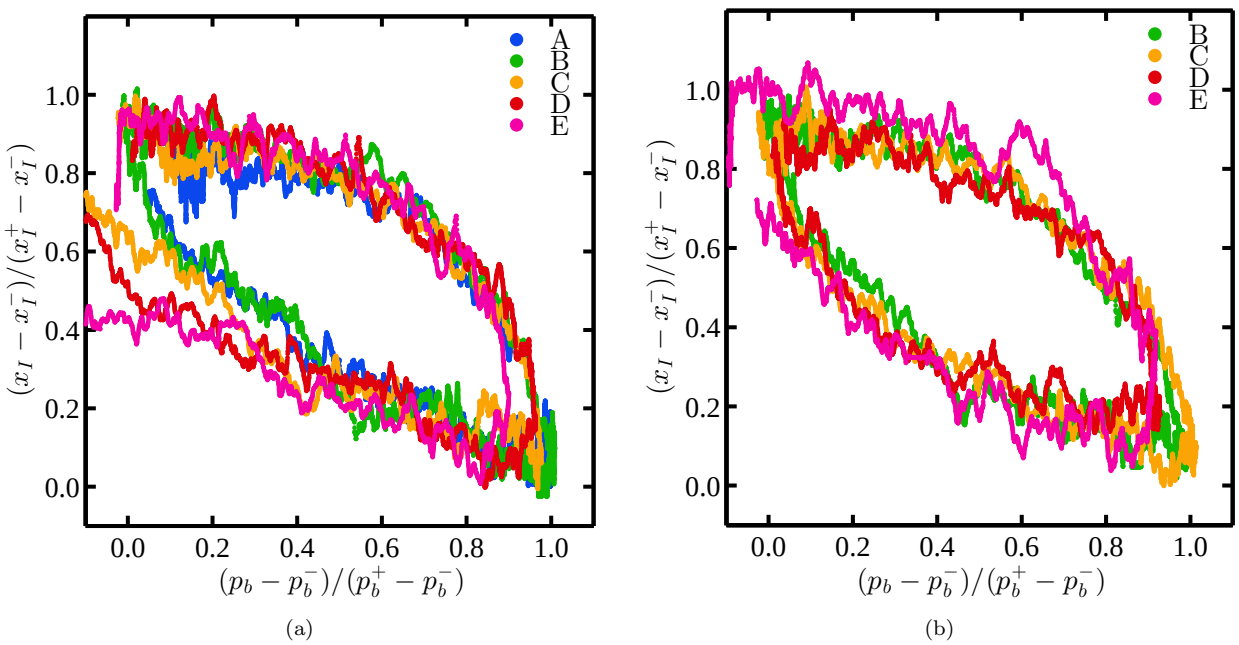

Figure 16. Shock position versus back pressure (normalized with the maximum and minimum values): (a) the first cycle for cases A-E; and (b) the second cycle of cases B-E.

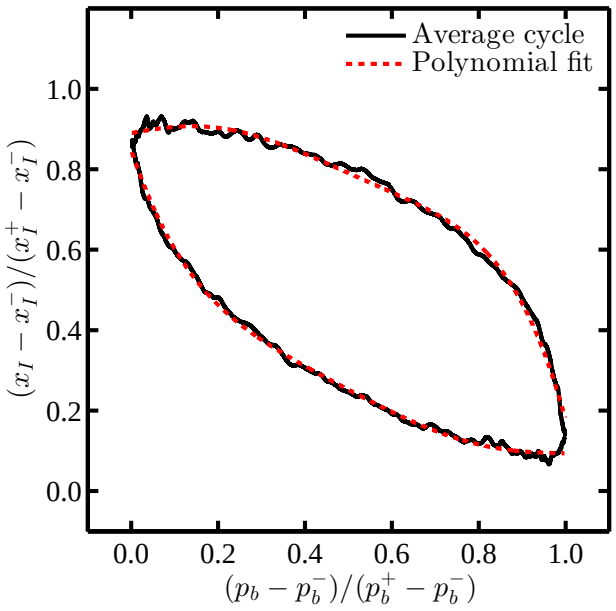

Figure 17. Average trajectory of the limit cycle across all of the cases (black line) and corresponding 4th order polynomial fit of the shock train trajectory (red line).

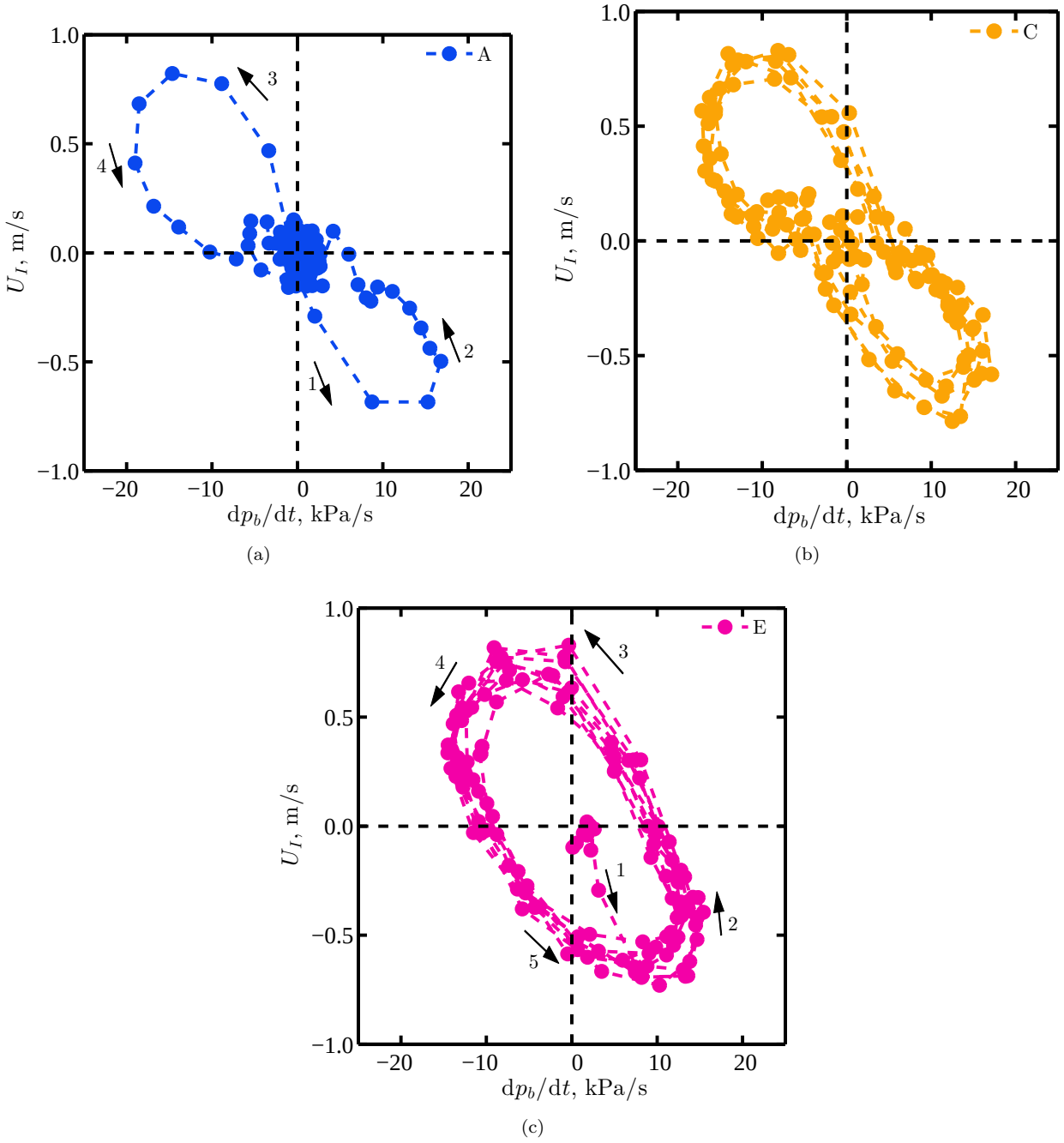

Figure 18. Bulk velocity component versus the back pressure rate of change: (a) case A; (b) case C; and (c) case E.